Penetration Estimation of GTAW with C-Type Filler by Net Heat Input Ratio

A novel method that considers arc efficiency was proposed to estimate the penetration in GTAW with filler metal

BY M. CHEEPU, H. J. BAEK, Y. S. KIM, AND S. M. CHO

Abstract

This study proposes a novel method to estimate the weld penetration in gas tungsten arc welding (GTAW) with filler metal. So far, there is no standard parameter available to accurately estimate penetration in GTAW with filler metal. Until now, the penetration could be estimated by heat input only in GTAW with and without filler metal. But in this study, it was revealed that the conventional heat input could not accurately estimate the penetration in GTAW with filler metal. Therefore, the new concept of net heat input ratio (NHIR), which is a ratio of net heat input to the bead cross-sectional area, was developed to accurately estimate the penetration in GTAW with filler metal. Using a C-type filler metal during GTAW, the NHIR was calculated for various welding conditions. The results showed that the NHIR was proportional to the welding current and voltage and inversely proportional to the welding speed and filler feed speed. Even though the NHIR was the same, the penetration increased as the welding current became higher. Four linear equations between NHIR and penetration were obtained from the experimental results for four levels of welding currents. By applying the concept of NHIR, the penetration could be estimated for any welding current.

Keywords

- Heat Input
- Welding Speed
- Filler Metal
- Deposition Rate
- Net Heat Input Ratio (NHIR)
- Fusion Depth
- Penetration
- Deposition Area
- Gas Tungsten Arc Welding (GTAW)
- C-Type Filler Metal

Introduction

In wire arc additive manufacturing (WAAM) or cladding, the fusion depth should be shallow and consistent. For the purpose of this paper, fusion depth shall be referred to as penetration. Gas tungsten arc welding (GTAW) is an excellent welding method for weld quality, but its productivity is inferior to other welding methods. Therefore, Cho et al. proposed a C-type filler metal to increase the deposition rate (DR), and thus the productivity, of GTAW (Ref. 1). Using the C-type filler metal during GTAW, high productivity and shallow penetration was obtained without a humping bead even in a high-current region and at a high DR (Ref. 2). This method can be effectively applied in the field of WAAM and cladding.

The penetration estimation is very important in effectively applying GTAW with C-type filler metal to WAAM and the cladding process. For the penetration estimation, it is necessary to establish the correlation between the heat input (HI) and filler feed speed (FFS) in GTAW with C-type filler metal.

https://doi.org/10.29391/2022.101.018

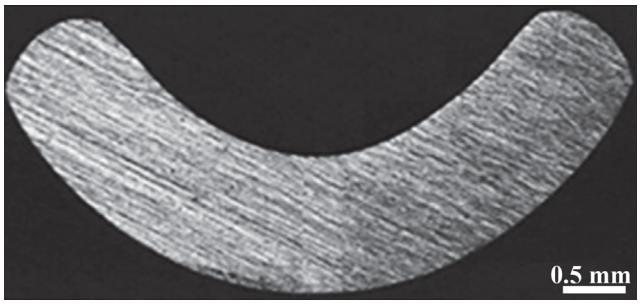

Fig. 1 — Cross-sectional view of the C-type filler metal.

Cho et al. defined the heat input ratio (HIR) with the HI and deposition area (DA) of the weld bead cross section (Ref. 3) as follows in Equation 1:

$$HIR = HI/DA \quad (1)$$

where HIR is the heat input ratio (J/mm^3), HI is the heat input (J/mm), and DA is the deposition area of the weld bead cross section (mm^2).

The HI and DA were calculated using Equations 2 and 3:

$$HI = (I \times E)/U \quad (2)$$

$$DA = (A_F \times FFS)/U \quad (3)$$

where I is the welding current (A), E is the voltage (V), U is the welding speed (mm/s), A_F is the cross-sectional area of the filler metal (mm^2), and FFS is the filler feed speed (mm/s).

The arc efficiency (η_a) should be considered for calculating the net heat input (NHI) because the arc efficiency is defined as the ratio of the energy absorbed by the workpiece to the energy supplied by the heat source (Refs. 4–6).

Therefore, the HIR in Equation 1 becomes the net heat input ratio (NHIR) by substituting the NHI for the HI.

In this paper, the correlation between the NHIR and penetration was clarified through quantitative experiments using GTAW with C-type filler.

Experimental Procedure

Base materials of ASTM A283 (SS440 steel) grade with a thickness of 10 mm (0.393 in.) were used in this study. Bead-on-plate welds were performed using ERNiCrMo-3 (Alloy 625) filler metal with a weld bead length of 100 mm (3.937 in.). The experiments were conducted as per the standard procedure of ISO/TR 18491, *Welding and allied processes — Guidelines for measurement of welding energies* (Ref. 7). The newly developed C-type filler (5 mm [0.196 in.] width, 1 mm [0.039 in.] thickness) was used for the experiments.

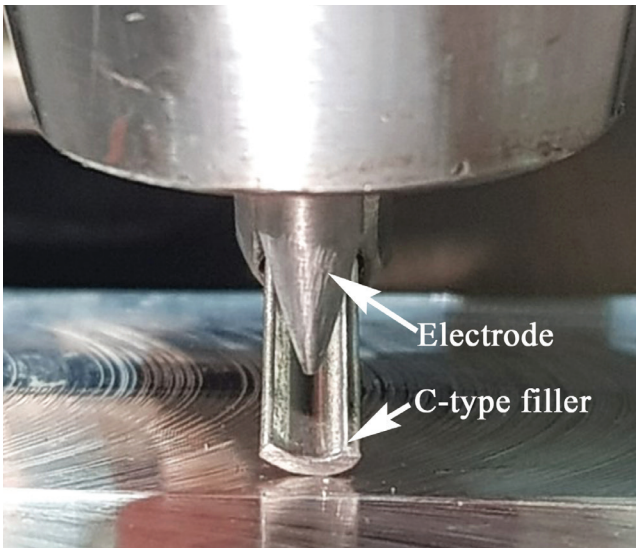

Fig. 2 — Front view of the C-type filler metal in GTAW.

The cross section of the C-type filler is shown in Fig. 1. The sectional area of the filler metal (A_F) was 5 mm^2. The experiments were performed using an industrial robot. The direct current GTAW welding machine (1000-A rated current) was used for direct current electrode negative (DCEN) polarity in the experiments. The 2% thoriated tungsten electrode with a diameter of 4 mm (0.157 in.) and a conical angle of 30 deg was conditioned before each experimental welding. The truncated tip diameter of the electrode changed with the welding current (I), such as 0.5 mm (0.019 in.) for 200 A, 1 mm for 300 A, 1.2 mm (0.047 in.) for 400 A, and 1.5 mm (0.059 in.) for 500 A, to obtain arc pressure stability and a uniformly welded joint (Ref. 8). Changing the tip diameter causes changes in arc pressure and possibly voltage (E) and introduces an uncontrolled variable that is not considered in the analysis for penetration.

Glickstein et al. (Ref. 9) reported the effect of the electrode tip configuration on voltage. The increase of the electrode tip flatness size causes a slight voltage reduction. The arc pressure is influenced by the electrode tip angle and its truncation. The heat from the arc to the substrate melts the substrate to a certain depth, but the arc pressure promotes a depression in the molten pool by accessing the heat flux to the molten metal that is deeper inside the substrate. The arc pressure distribution for the sharp electrode tips is a steep Gaussian. The arc pressure distribution is rectangular for the blunt electrode tips that have flat ends with a lower maximum (Ref. 10). In addition, flat ends are considered to prevent tungsten inclusion defects in welds. The shielding gas mixture of Ar + 7%H_2 was used with a gas flow rate of 20 L/min (42.37 ft^3/h). The arc length (in cold conditions) was 5 mm, and it was determined as the stand-off distance between the electrode tip and workpiece before welding. The feeding angle of the filler metal was 20 deg from the base metal, and its position with the electrode is exhibited in Fig. 2.

The output voltage was measured for all the experimental welds by the GTAW waveform monitor (see Table 1). The welding experiments were conducted at four different welding currents: 200, 300, 400, and 500 A. The experimental

Table 1 — Welding Parameters of GTAW with C-Type Filler Metal (200~500 A)

Current (A)	DR (kg/h)	FFS (cm/min)	Welding Speed (cm/min)					
			20		40		60	
			DA (mm^2)	Voltage (V)	DA (mm^2)	Voltage (V)	DA (mm^2)	Voltage (V)
	1	40	10	18.92	5	20.78	—	—
	1.5	60	15	18.51	7.5	20.48	—	—
200	2	80	20	18.41	10	20.25	—	—
	2.5	100	25	18.31	12.5	20.10	—	—
	3	120	30	18.19	15	19.91	—	—
	3.5	140	35	17.74	17.5	19.65	—	—
	2	80	20	19.96	10	20.25	6.67	20.36
	2.5	100	25	19.35	12.5	20.19	8.33	20.31
300	3	120	30	19.01	15	19.82	10.00	20.23
	3.5	140	35	18.91	17.5	19.67	11.67	20.14
	4	160	40	18.77	20	19.36	13.33	19.80
	4.5	180	45	18.25	22.5	19.34	15.00	19.76

Table 1 — (continued)

Current (A)	DR (kg/h)	FFS (cm/min)	Welding Speed (cm/min)					
			20		40		60	
			DA (mm^2)	Voltage (V)	DA (mm^2)	Voltage (V)	DA (mm^2)	Voltage (V)
	5	200	50	19.99	25	20.76	16.67	21.59
	6	240	60	19.52	30	20.56	20.00	21.23
400	7	280	70	19.32	35	20.37	23.33	20.80
	8	320	80	19.21	40	20.26	26.67	20.52
	9	360	90	19.13	45	20.18	30.00	20.26
	7	280	70	22.05	35	22.37	23.33	22.83
	8	320	80	21.98	40	22.22	26.67	22.58
500	9	360	90	21.29	45	21.89	30.00	21.97
	10	400	100	21.06	50	21.60	33.33	21.62
	11	440	110	20.89	55	21.18	36.67	21.53
	12.1	480	120	20.72	60	20.99	40.00	21.23

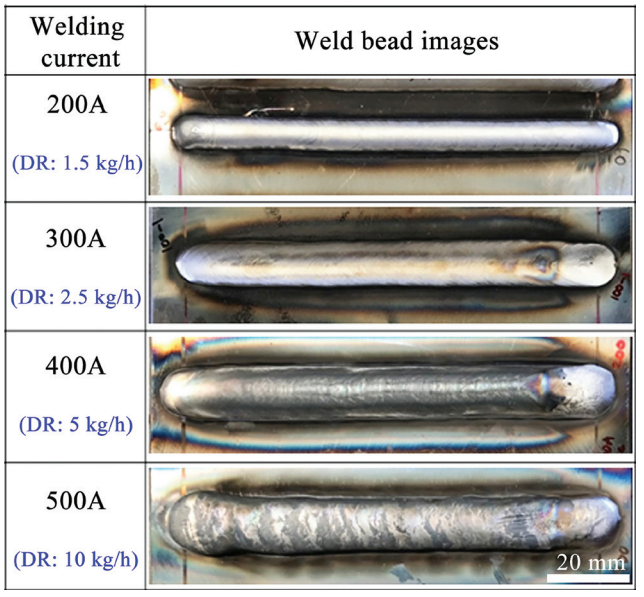

Fig. 3 — Weld bead appearance at different welding currents (welding speed 20 cm/min).

details are given in Table 1. For each welding current, different welding speeds (U) were used. Moreover, different FFSs were applied for each welding speed. The FFS was used to obtain the DA and DR of the weld beads (Ref. 3). The DA of the weld bead cross sections was calculated using Equation 3, assuming a 100% capture efficiency. The DA is above the original surface and can be calculated before welding. Referencing Jenney and O'Brien as well as Dupont and Marder, the NHIR and NHI were calculated using arc efficiency (Refs. 4, 5). The new concept of NHIR, which is a product of η_a and HIR, or the ratio of NHI to DA, was calculated using Equation 4:

$$NHIR = \eta_a \times HIR = NHI/DA \quad (4)$$

The NHI was calculated using Equation 5:

$$NHI = \eta_a \times HI \quad (5)$$

where the HI was calculated using a set welding current, measured voltage, and current-adjusted process efficiency as discussed later; NHIR is the net heat input ratio (J/mm^3); NHI is the net heat input (J/mm); and η_a is the arc efficiency.

The welds were cross sectioned and polished for macrosectional analysis to measure the penetration. To reveal the penetration, the polished surfaces were etched with 4% Nital solution. The penetration was measured using an image measuring software. The largest distance of fusion extending into the base metal from the surface that melted during welding was used as the penetration value. Penetration measurements were calculated from three cross sections

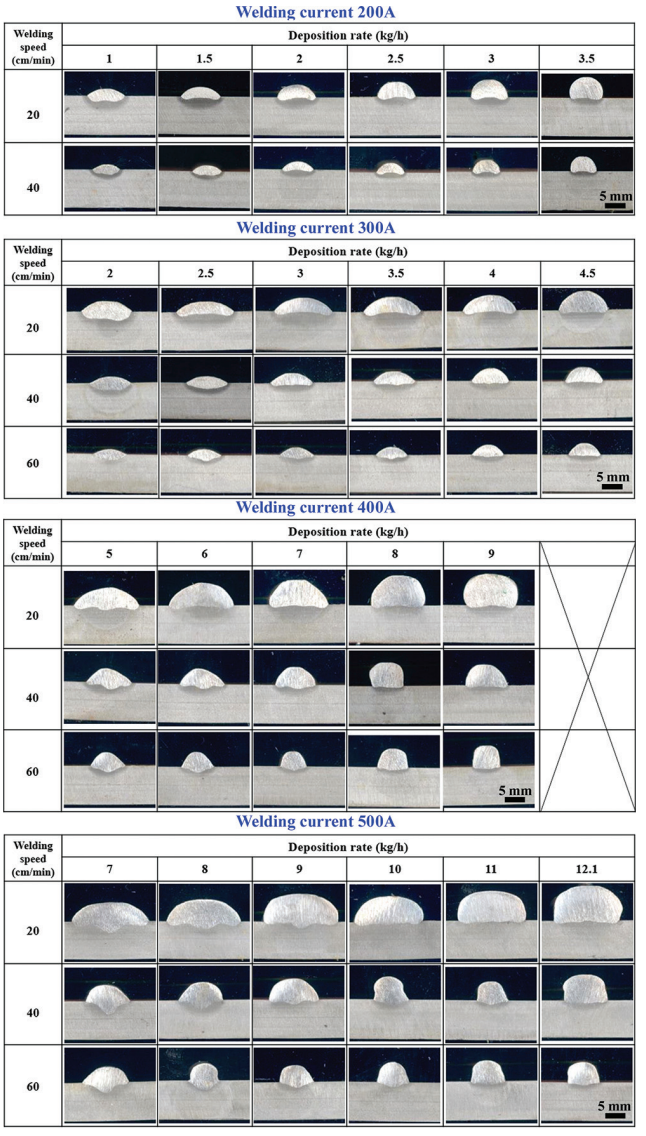

Fig. 4 — Macrosection of the weld beads at welding currents of 200~500 A.

of the weld bead, and the average values for each welding condition were taken.

Results and Discussion

Weld Bead Appearance

Each DR was kept constant for each welding speed at 20, 40, and 60 cm/min (7.87, 15.74, and 23.62 in./min), and the welds were performed with different deposition areas (details shown in Table 1). In the case of the 200-A welding current, travel speeds of 20 and 40 cm/min were used due to the maximum limit of welding speed (see Table 1).

Figure 3 shows the weld bead appearance obtained at different welding currents for the same welding speed of

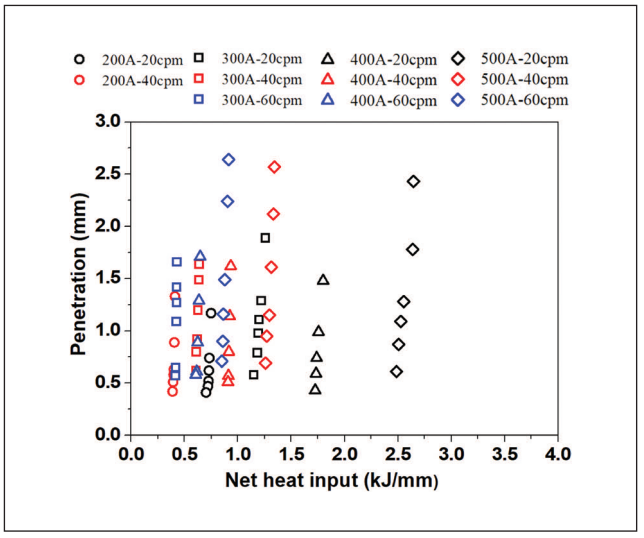

Fig. 5 — Penetration according to the NHI in GTAW with filler metal at various welding currents (I) and welding speeds (U). The FFS was varied for each combination of the I and U (as per Table 1).

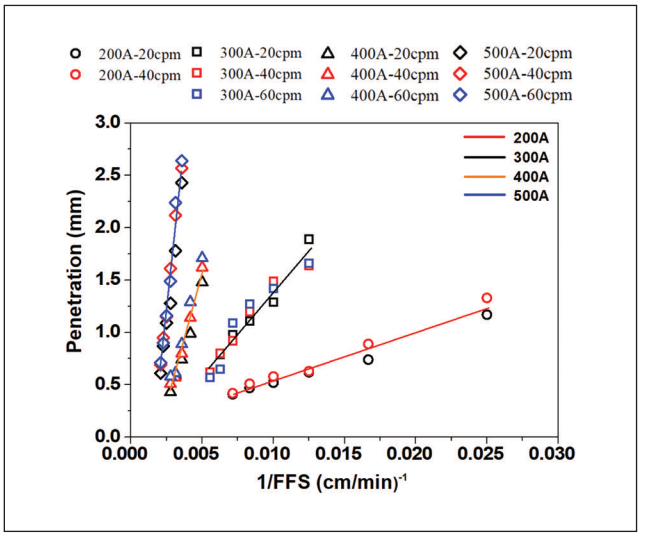

Fig. 6 — The effect of 1/FFS on penetration at various welding currents and welding speeds. The FFS is taken in fractional numbers (1/FFS) to represent its linear relation with penetration.

20 cm/min. The DRs for each welding current were different because the FFS changed.

In this study, adequate penetration was considered above 0.3 mm (0.01 in.) and below 3 mm (0.11 in.) without tunnel defects, undercuts, or humping bead defects. Incomplete fusion and incomplete joint penetration may occur below 0.3 mm in penetration, and more than 3 mm is not required in WAAM and cladding.

Macrosection of the Welds

Weld macrosections at different welding currents (200~500 A) are illustrated in Fig. 4. The welds produced with a DR of 1~3.5 kg/h (2.2~7.7 lb/h) used a welding current of 200 A, and the welding speed changed with the FFS. The penetration and weld shape changed with the increase of the DR. Welds with a 1 kg/h DR showed deeper penetration over welds with a 3.5 kg/h DR. In addition, the weld shape also varied from semicircular (1 kg/h DR) to a hemisphere (3.5 kg/h DR). In the case of the 300-A welding current, welds were produced with a DR of 2~4.5 kg/h (4.4~9.9 lb/h). Even though the DR was the same, the weld bead cross-sectional area decreased with the increase of welding speed. Therefore, the penetration and shape of the welds gradually changed. At the same time, this trend was slightly affected by the DR. The DR of 5~9 kg/h (11~19.8 lb/h) was obtained with the 400-A welding current. The weld beads formed initially with a convex shape like a finger-type profile with deep and narrow penetration. The finger-type weld bead gradually disappeared by changing its width and height as the DR increased. Also, the finger-type weld bead profiles started to appear as the welding current increased to 400 A. In the case of the 500-A welding current, there were finger-type weld beads until the deposition rate of 9 kg/h. After that, they disappeared and changed the penetration shape, as shown in Fig. 4. The maximum deposition rate of 12 kg/h (26.4 lb/h) can be obtained with desirable penetration and quality.

Relation between NHI and Penetration

Figure 5 shows the relation between NHI and penetration. The experimental results obtained at welding currents of 200, 300, 400, and 500 A with three different welding speeds and various FFSs (see Table 1) were used to plot the graph. Even though the NHI was the same, the penetration varied by the FFS. Hui et al. proposed that the NHI is a governing factor in controlling the penetration in GTAW with and without filler metal (Ref. 11). However, Fig. 5 shows that even though the welding current and NHI were the same, penetration increased as the FFS decreased (see Table 1). Penetration is governed more significantly by the FFS (in the same welding current) and the welding current than the NHI. Therefore, penetration estimation using the NHI alone is inaccurate in GTAW with filler metal.

The HI is proportional to the welding current and voltage and inversely proportional to the welding speed. As per Dupont and Marder (Ref. 12), the heat effects of the arc on the material being welded are considered different compared to the theoretical heat. Therefore, the NHI was also calculated using arc efficiency, as given in Equation 5. The NHI was determined using the arc efficiency during GTAW according to the welding current (Refs. 4, 12). However, these studies have only reported arc efficiency data up to 350 A for GTAW. Welding currents above 350 A are extrapolated using available (below 350 A) data. The relation between the welding current and arc efficiency was determined using the linear regression equation in Equation 6:

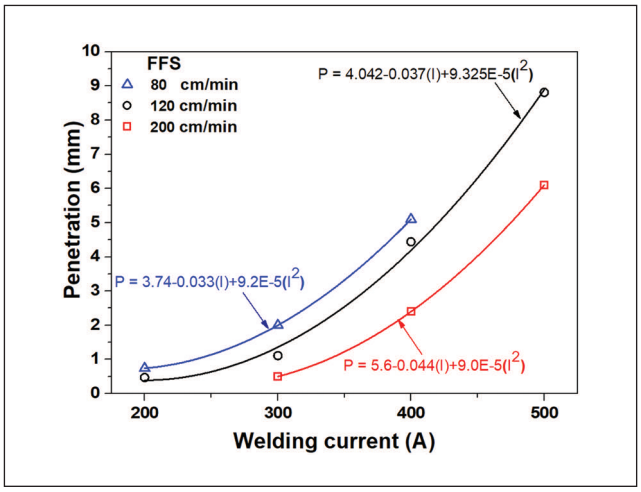

Fig. 7 — The effect of the welding current on penetration at different FFSs.

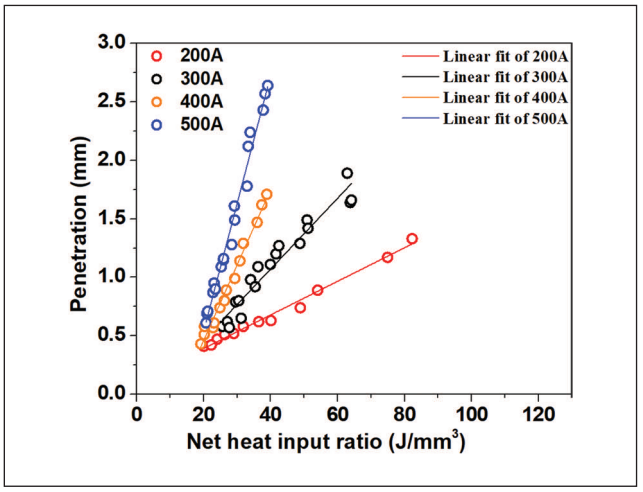

Fig. 8 — The comparison graph shows the relation between the NHIR and penetration at different welding currents.

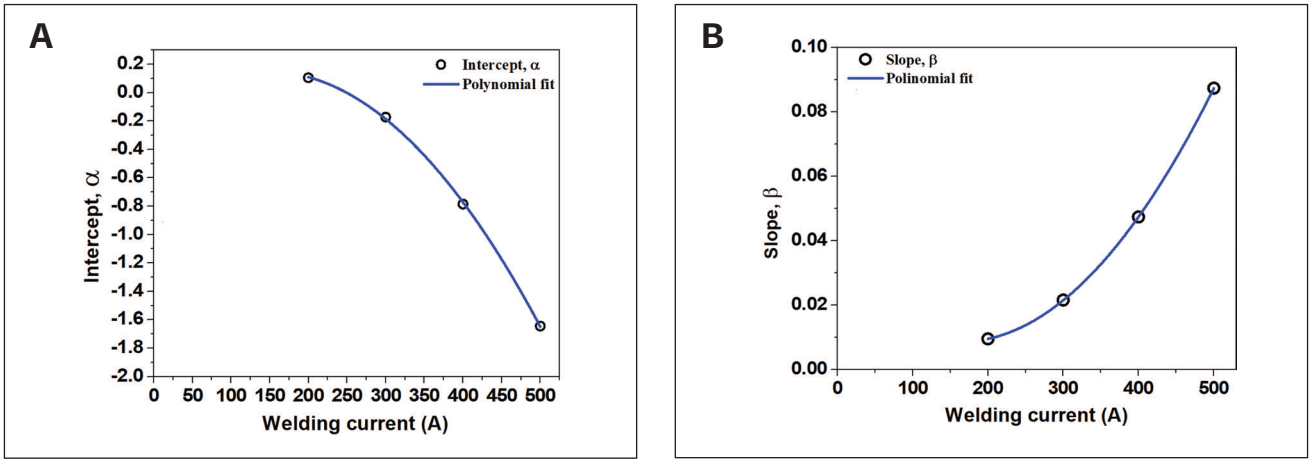

Fig. 9 — Polynomial fitting curves for intercept α (A) and slope β (B) of the linear fitted graphs of four different welding currents (based on the data from Fig. 8).

$$\eta_a = (I \times 0.00045) + 0.54 \quad (6)$$

where η_a is the arc efficiency and I is the welding current (A).

The required arc efficiency was calculated for welding currents of 200, 300, 400, and 500 A using Equation 6. The obtained arc efficiency using Equation 6 was 0.63 for 200 A, 0.68 for 300 A, 0.72 for 400 A, and 0.77 for 500 A. The NHI and NHIR were calculated using these arc efficiency values to estimate penetration. The quality of the results improved using η_a rather than HIR because it better fits the relation between penetration and the NHIR.

It seems that the conventional NHI parameter is suitable for predicting the penetration only at a constant DA. This study also identified that the arc voltage decreased when the FFS increased because the reinforcement height increased and the distance (arc length) from the electrode tip to the top of the weld bead decreased. The voltages varied for welds made at the same welding speed and DR, as given in Table 1. At the same welding speeds, different FFSs were used for welding. Increasing the FFS at the same welding speed increased the DA (as per Equation 3). The melting/weld bead width was almost the same or possibly reduced due to less arc energy to melt the base metal when increasing the FFS. Thus, the reinforcement height increased with the increase of the DA or FFS, and the arc length and voltages decreased. Correspondingly, at the same DRs (same FFS), welding speeds increased from 20 to 60 cm/min. The increase in welding speed reduced the DA (as per Equation 3). Hence, the reinforcement height decreased with the decrease of the DA, and the arc length and voltages increased. The voltage variation by changing arc length was reported elsewhere (Refs. 9, 13). Therefore, it was only possible to get the HI after welding. At the same time, it is possible to predict prior to welding if the automatic voltage controller used during welding can maintain constant voltage.

Figure 6 represents the relation between the FFS and penetration at different combinations of welding current and welding speed. The penetration is proportionally linear to 1/FFS in the same welding current even with varying welding speeds. The NHI of the welds at the same welding current and speed is the same, but penetration varies by FFS. However, as shown in Fig. 6, penetration also changes with the welding current.

Figure 7 shows that the penetration varied by welding current I^2 at the same FFS. Thus, the penetration is governed by 1/FFS and welding current I^2. Rokhlin and Guu (Ref. 14) reported the effect of the welding current on penetration and weld pool depth. Both varied with the increasing welding current. The penetration and weld pool depth rose slowly in the current range of 100 to 250 A and improved above 250 A due to increased arc force because the arc force is proportional to I^2. Equation 7 clarifies the effect of the FFS and welding current on penetration. The relation between penetration and NHIR is discussed in the following section. NHIR is described with I, E, A_F, and FFS functions in Equation 7 (which is derived from Equation 4):

$$NHIR = \eta_a(I \times E)/(FFS \times A_F) \quad (7)$$

In Equation 7, the welding current as a dividend and FFS as a divisor result in a different effect on the penetration.

Relation between NHIR and Penetration

The HIR parameter involved the welding current, voltage, welding speed, and weld bead cross-sectional area (Refs. 3, 15). It was developed for the estimation of penetration in GTAW with filler metal. In the HIR, arc efficiency was not involved, but penetration can be affected by arc efficiency. Consequently, arc efficiency and HIR are considered in the NHIR, as seen in Equation 4. The use of the NHIR revealed a better relation with penetration. The NHIR parameter was calculated for different welding conditions to predict penetration in GTAW with filler metal. The bead cross-sectional area was proportional to the FFS. As the bead cross-sectional area increased, the arc length started to decrease; therefore, the voltage also decreased.

Figure 8 shows the relation between NHIR and penetration at 200~500 A with different welding speeds and FFSs. It was observed that the NHIR is proportional to the welding current and voltage and inversely proportional to the welding speed and FFSs. The one linear relation between the NHIR and penetration was obtained with the same welding current even though the welding speed changed. In the same NHIR, if the welding current increased, penetration also increased. For 40 J/mm^3 NHIR, the penetration was 0.5 mm (0.019 in.) for 200 A, whereas at the same NHIR value (40 J/mm^3), the penetration was 1.7 mm (0.067 in.) for 500 A. Using the NHIR and welding current, it is possible to estimate penetration accurately, and the relation between the NHIR and penetration resulted in an excellent linear fitting for four levels of welding currents: 200, 300, 400, and 500 A. Similar trends in the NHIR can be obtained using round wire, except that humping defects occurred with currents above 400 A. In addition, penetration can be estimated for any welding current with different welding speeds and weld bead cross-sectional areas using the experimental data for the four welding currents. The linear fitted curves were obtained for the four currents, as shown in Fig. 8. Four different equations were derived from the four linear fitted curves. The single linear curve of Equation 8 was obtained from four linear curves (see Fig. 9) to estimate penetration for any welding current in the range of 200~500 A. Penetration for any welding current can be estimated using Equation 9. The relation between the NHIR and penetration is evident and confirms that the NHIR accurately estimates the penetration in GTAW with filler metal.

$$P = \alpha + \beta(NHIR) \quad (8)$$

where P is the penetration (mm), α is the intercept, β is the slope, and NHIR is the net heat input ratio (J/mm^3).

$$\begin{aligned} P = {} & -0.11 + 0.00400(I) - 1.4203 \times 10^{-5}(I^2) \\ & + \left(0.02342 - 1.9476 \times 10^{-4}(I) + 7.5175 \times 10^{-7}(I^2)\right) \\ & \times ((\eta_a \times I \times V)/(FFS \times A_F)) \end{aligned} \quad (9)$$

The NHI and NHIR can be calculated by setting four variables: the current, the voltage using an automatic voltage controller (AVC), the welding speed, and the feed speed of the C-type filler metal. In GTAW, voltage usually is a variable dependent on current and arc length, etc. But it was recently discovered that the set voltage could be obtained automatically by the AVC through arc length controlling. Hence, penetration can be estimated before performing welds using the NHIR, which is calculated by using the four variables.

Conclusions

To estimate the penetration in WAAM and cladding by GTAW with a C-type filler metal, the NHIR parameter was defined and used. Welding currents of 200, 300, 400, and 500 A were applied to obtain the DR of 1 to 12 kg/h. Penetration of 0.3 to 3.0 mm was considered useful for good welding quality.

The conclusions are as follows:

1) Even though the welding current and NHI in regards to arc efficiency were the same, if the FFS increased, penetration decreased. Therefore, it was difficult to estimate penetration using only the NHI in GTAW with filler metal.

2) Penetration was proportionally linear to 1/FFS in the same welding current. Also, it was proportional to the welding current I^2 with the same FFS.

3) The NHIR was proportional to the welding current and voltage, but it was inversely proportional to the welding speed and FFS. The one linear relation between the NHIR and

penetration was obtained with the same welding current even though the welding speed and FFS changed.

4) In the same NHIR, if the welding current increased, penetration also increased. Therefore, a different equation between the NHIR and penetration was used for different welding currents.

5) The penetration could be estimated using the novel concept of the NHIR for any welding current in the range of 200~500 A and DRs in the range of 1~12 kg/h.

Acknowledgments

This research was supported by the Korea Evaluation Institute of Industrial Technology (KEIT), Daegu, South Korea, under the Ministry of Trade, Industry and Energy (MOTIE), South Korea, Grant No. 20004932.

References

1. Cho, S.-M., Oh, D.-S., Ham, H.-S., Ha, H.-J., Shin, H.-S., Jun, J.-H., Byun, J.-G., Park, J.-H., and Kwon, H.-Y. 2016. Filler metal for TIG welding, U.S. Patent US20160199947A1.

2. Jun, J. H., Park, J. H., Cheepu, M., and Cho, S. M. 2020. Observation and analysis of metal transfer phenomena for high-current super-TIG welding process. *Science and Technology of Welding and Joining* 25(2): 106–111. DOI: 10.1080/13621718.2019.1637172

3. Park, J. H., Cheepu, M., and Cho, S. M. 2020. Analysis and characterization of the weld pool and bead geometry of Inconel 625 Super-TIG welds. *Metals* 10(3): 365. DOI: 10.3390/met10030365

4. Jenney, C. L., and O'Brien, A., eds. 2001. "Chapter 3 — Heat Flow in Welding." In *Welding Handbook,* Welding Science and Technology, Vol. 1, 9th Ed. Miami, Fla.: American Welding Society.

5. DuPont, J. N., and Marder, A. R. 1996. Dilution in single pass arc welds. *Metallurgical and Materials Transactions B* 27(3): 481–489. DOI: 10.1007/BF02914913

6. Crement, D. J. 1993. Narrow groove welding of titanium using the hot-wire gas tungsten arc process. *Welding Journal* 72(4): 71–76.

7. ISO/TR 18491, *Welding and allied processes — Guidelines for measurement of welding energies*. 2015. Geneva, Switzerland: International Organization for Standardization.

8. Fukuhisa, M., Ushio, M., and Kumagai, T. 1986. Study on gas-tungsten-arc electrode (Report 1): Comparative study of characteristics of oxide-tungsten cathode (welding physics, process & instrument). *Transactions of JWRI* 15(1): 13–19.

9. Glickstein, S. S., Friedman, E., and Yeniscavich, W. 1975. Investigation of Alloy 600 welding parameters. *Welding Journal* 54(4): 113-s to 122-s.

10. Alber, A. S., Ushio, M., and Fukuhisa, M. 1987. Gas-tungsten-arc cathode and related phenomena. *Transactions of JWRI* 16(1): 195–210.

11. Hui, H., Yin, X., Feng, Z., and Ma, N. 2019. Finite element analysis and in-situ measurement of out-of-plane distortion in thin plate TIG welding. *Materials* 12(1): 141. DOI: 10.3390/ma12010141

12. DuPont, J. N., and Marder, A. R. 1995. Thermal efficiency of arc welding processes. *Welding Journal* 74(12): 406-s to 416-s.

13. Burgardt, P., and Heiple, C. R. 1992. Weld penetration sensitivity to welding variables when near full joint penetration. *Welding Journal* 71(9): 341-s to 347-s.

14. Rokhlin, S. I., and Guu, A. C. 1993. A study of arc force, pool depression, and weld penetration during gas tungsten arc welding. *Welding Journal* 72(8): 381-s to 390-s.

15. Jenney, C. L., and O'Brien, A., eds. 2001. "Chapter 10 — Monitoring and Control of Welding and Joining Processes." In *Welding Handbook,* Welding Science and Technology, Vol. 1, 9th Ed. Miami, Fla.: American Welding Society.

MURALIMOHAN CHEEPU (*muralicheepu@gmail.com*; *mmcheepu@super-tig.kr*), **HYO JIN BAEK**, **YOUNG SIK KIM**, and **SANG MYUNG CHO** are with Super-TIG Welding Co. Ltd., Busan, Republic of Korea.